Diffusive Motions Control the Folding and Unfolding Kinetics of the Apomyoglobin pH 4 Molten Globule Intermediate†

Carlos H. I. Ramos,‡ Sebastien Weisbuch,§ and Marc Jamin*,‖

Laboratório Nacional de Luz Síncrotron, P.O. Box 6192, Campinas SP 13084-971, Brazil, ImmunID, CEA/DRDC, 17 rue des Martyrs, 38057 Grenoble Cedex 9, France, and Unit of Virus Host Cell Interactions, UMR 5233, UJF-EMBL-CNRS, 6 rue Jules Horowitz, B.P. 181, 38042 Grenoble Cedex 9, France

Received December 15, 2006; Revised Manuscript Received February 14, 2007

ABSTRACT: The sperm whale apomyoglobin pH 4 folding intermediate exists in two forms, Ia and Ib, that mimic transient kinetic intermediates in the folding of the native protein at pH 6. To characterize the nature of the kinetic barrier that controls the formation of the earliest intermediate Ia, we have investigated the effects of small viscogenic cosolvents on its folding and unfolding kinetics. The kinetics are measurable by stopped-flow fluorescence and follow a cooperative two-state model in the absence and presence of cosolvents. Small cosolvents stabilize Ia, but, by applying the isostability test to separate the viscogenic effect of the cosolvent from its stabilizing effect, we found that, in both folding and unfolding conditions, the apparent rate constant decreases when solvent viscosity increases. The unitary inverse dependence of the apparent rate constant on solvent viscosity indicates a diffusion-controlled reaction. This result is consistent with the hypothesis that folding of the apomyoglobin pH 4 intermediate obeys a diffusion-collision model. Additionally, the temperature dependence of the reaction rate at constant viscosity indicates that the formation of Ia is also controlled by an energy barrier. Linear free energy relationships show that the transition state of the U ⇌ Ia reaction is compact and buries 45% of the surface area that is buried in native apomyoglobin. We conclude that the transition state of the U ⇌ Ia reaction resembles that for the formation of native proteins; namely, it is dry and its compactness is closer to that of the folded (Ia) form than of the unfolded form.

In the earliest times of protein folding reactions, the polypeptide chain must undergo motions in solution in order to collapse into compact states, to form secondary structures and to find its native topology. The nature of the kinetic barriers that control these reactions is still not completely understood (*1*). Thirty years ago, the importance of diffusive motions in controlling the rate of folding reactions was underlined in the diffusion-collision model (*2*). Studies with peptides and model proteins show that secondary structure formation and chain collapse occur extremely rapidly in isolation (*3*−*12*) and are limited in rate by diffusion (*3*, *6*, *12*−*14*). However, how the dynamics of these processes are coupled in the early stages of protein folding is difficult to assess experimentally.

Many single domain proteins of more than 100 amino acids fold in two stages, rapidly forming partially structured kinetic intermediates that convert more slowly into native forms (*15*−*19*). In some cases, similar intermediates also exist at equilibrium under particular conditions (*20*−*22*). The formation of kinetic or equilibrium intermediates from unfolded proteins represents good models to investigate how elementary processes such as secondary structure formation and chain collapse are coupled in the early stages of folding reactions.

In recent years, Kramers' theory appears well suited for modeling protein folding reactions and in particular to account for the observed viscosity dependence of folding rates (*1*, *23*−*27*). According to this theory, unimolecular folding reactions are limited in rate both by the height of an energy barrier and by friction of protein groups against solvent molecules or against other protein groups. For reactions dominated by solvent friction, Kramers' theory predicts an inverse dependence on solvent viscosity, while for reactions dominated by internal friction, it predicts independence on solvent viscosity. A general equation accounting for these limiting cases has been proposed (*26*, *28*−*30*):

$$k = \frac{\gamma}{\eta + \sigma} \exp\left(\frac{-\Delta G^{\circ\ddagger}}{RT}\right) \quad (1)$$

where η is the solvent viscosity, σ is the corresponding term for internal friction, $\Delta G^{\circ\ddagger}$ is the free energy barrier, and γ is the proportionality constant. Internal friction limits motions in very short peptides (*31*) and folding of small proteins at infinitely low viscosity (*28*, *32*). However, in the high friction limit of water solutions, theoretical studies predict an inverse dependence of folding rates on solution viscosity (*33*, *34*),

†This work was supported by a visiting professor fellowship from the Université Joseph Fourier of Grenoble to C.H.I.R., who also thanks Fundação de Amparo do Estado de São Paulo FAPESP and Conselho Nacional de Desenvolvimento Científico e Tecnológico CNPq.

* Corresponding author. E-mail: jamin@embl.fr. Phone: +33 4 76 20 94 62. Fax: +33 4 76 20 94 00.

‡ Laboratório Nacional de Luz Síncrotron.

§ ImmunID.

‖ Unit of Virus Host Cell Interactions (UVHCI).

10.1021/bi602574x CCC: $37.00
Published on Web 03/17/2007

and experimental studies show such dependence for different folding reactions, including the formation of isolated α-helix and β-hairpin in synthetic peptides (*13*), the docking and folding of ribonuclease S-peptide on structured S-protein (*35*), the assembly and folding of small dimeric proteins (*25*, *36*), the overall folding of small monomeric proteins that fold rapidly without accumulating intermediate (*29*, *30*, *37*, *38*), and the late assembly of domains in large multidomain proteins (*39*−*42*). Control by diffusive motions was also demonstrated for the folding of the α-spectrin SH3 domain by the effect of glycine loop insertion on the folding rate (*43*). All these diffusion-controlled reactions occur on very different time scales, ranging from microseconds to hours, as predicted by Kramers' theory for different heights of the energy barrier (*24*).

Sperm whale apomyoglobin folds to its native conformation (N) at pH 6 by transiently populating at least two different partially structured intermediates, named here Ia and Ib (*20*, *44*). Although no formal evidence has been obtained, available structural and kinetic information suggests that at least one of these intermediates is on the folding pathway (*20*, *44*−*46*). The formation of the earliest intermediate, Ia, is too fast to be monitored even with the fastest mixing device, but similar partially structured forms of the protein exist as stable intermediates at equilibrium near pH 4 in low salt conditions (*44*, *47*−*49*). In these conditions, both Ia and Ib coexist (*44*), and thus equilibrium measurements report on the mixture of both species that are collectively named I.[1] These stable pH 4 forms serve as models for exploring the properties of the more relevant kinetic intermediates observed at pH 6. The structure of the protein at pH 4 has been extensively characterized by site-directed mutagenesis, hydrogen exchange, NMR spectroscopy, or SAXS (*50*−*56*), and the relationship between equilibrium and kinetic intermediates has been firmly established (*20*, *56*). Both kinetic and equilibrium intermediates are compact with a structured core formed by the A, H, and G helices of myoglobin (Mb) as well as by a part of the B helix and with a loosely packed central region that contains fluctuating D and E helices (*20*, *47*, *50*, *54*). Interestingly, at pH 4.2 in low salt conditions, folding and unfolding kinetics of Ia are measurable in the millisecond time range within its urea-induced unfolding transition (*44*, *57*−*59*). This folding process exhibits many features of a two-state, highly cooperative reaction in which the hydrophobic core and some elements of native secondary structure are formed in a few milliseconds (*57*, *59*). The reaction is, however, complicated by the presence of the second intermediate, Ib, but problems are avoided by working within the transition region, above 1 M urea, where Ib is lowly populated and unfolds very quickly (*44*). The formation of Ia at pH 4.2 is thus an excellent model for investigating the nature of an early protein folding kinetic barrier.

We report here the effects of small viscogenic cosolvents, such as sucrose and glycerol, on the structure, the stability, and the folding and unfolding kinetics of the apoMb intermediate Ia at pH 4.2. Measuring the effects of solvent viscosity on the folding and unfolding reactions is difficult because small viscogenic cosolvents also modify protein stability (*60*). A test was devised for separating the viscogenic and stabilizing effects (*40*) and is applied here. The properties of the transition state for the U ⇌ Ia reaction are then discussed on the basis of linear free energy relationships established for denaturing (urea) and stabilizing (sucrose and glycerol) cosolvents.

MATERIALS AND METHODS

Urea, sucrose, glycerol, sarcosine, and TMAO were purchased from Sigma. All experiments were performed in 2 mM sodium citrate and 30 mM NaCl at pH 4.2 and at 5 °C.

Sperm whale apoMb was produced and purified as previously described (*59*). Protein solutions were prepared in distilled water, filtered, and dialyzed extensively against distilled water. Protein concentration was determined by absorbance in 6.0 M GdmCl (20 mM sodium phosphate, pH 6.5) as described (*61*), using $\epsilon_{280nm} = 15200\ M^{-1}\ cm^{-1}$ and $\epsilon_{288nm} = 10800\ M^{-1}\ cm^{-1}$.

Spectroscopic Measurements. CD spectra were measured on a Jasco (Tokyo) J810 spectropolarimeter using a thermostated quartz cell. A protein concentration of 10 μM and path length of 1 mm were used for far-UV CD spectra. A protein concentration of 100 μM and path length 10 mm were used for near-UV CD spectra. Emission fluorescence spectra were measured on a Jasco (Tokyo) FP6200 spectrofluorometer using a 1 cm quartz cell. Excitation was set at 288 nm.

One-dimensional ^1H spectra were acquired in 10% D_2O at 25 °C on a Varian INOVA 600 spectrometer, using 4096 complex points over a spectral width of 10000 Hz. For protein samples without sucrose, water suppression was achieved by using a Watergate sequence (*62*). For samples containing 0.5 or 1.0 M sucrose, two spectra were recorded using sculpting sequences with a selective excitation on methyl groups (pulse of 592 μs, 4 ppm wide, centered on −0.5 ppm) or on amide groups (pulse of 592 μs, 4 ppm wide, centered on 9.5 ppm) (*63*). Solutions of 100 μM sperm whale apoMb were prepared in the absence or presence of sucrose in 5 mM acetate buffer, pH 4.2 or 5.7, and 10% D_2O.

Stopped-Flow Experiments. Folding and unfolding kinetics were measured by Trp fluorescence with a SFM-4 stopped-flow instrument (Bio-Logic, Claix, France). The excitation was set at 288 nm, and the emission was detected at 90°, using an optical cutoff filter (50% transmittance at 305 nm). The curves were fitted to a single exponential function by using the software provided by Bio-Logic. The efficiency of mixing and the dead-time were estimated in the absence and presence of 1 M sucrose by using a fluorescence quenching reaction between *N*-acetyltryptophanamide and *N*-bromosuccinamide (*64*). The efficiency of mixing was estimated by monitoring fluorescence intensity when the liquid flows through the observation cell before the stop. In the absence or in the presence of 1 M sucrose, the fluorescence intensity increases and reaches a plateau during the mixing time, indicating that mixing is complete. The dead time measured in both conditions was smaller than 1 ms.

[1] Abbreviations: apoMb, apomyoglobin (myoglobin without the heme group); CD, circular dichroism; I, intermediate; LEM, linear extrapolation method; NMR, nuclear magnetic resonance; TMAO, trimethylamine *N*-oxide.

Data Analysis. Equilibrium and kinetic data were analyzed with a two-state model:

$$U \underset{k_{21}}{\overset{k_{12}}{\rightleftharpoons}} I_a \quad (2)$$

where k_{12} is the folding rate constant and k_{21} is the unfolding rate constant. The equilibrium constant for unfolding is defined as

$$K = [U]/[Ia] = k_{21}/k_{12} \quad (3)$$

and the apparent rate constant obtained by integrating the rate equation is given by

$$\lambda = k_{12} + k_{21} \quad (4)$$

Within the urea-induced unfolding transition, standard relationships are used for the dependences of the free energies on urea concentration (*65*):

$$\Delta G^\circ = \Delta G^\circ(H_2O) - m_{urea}[urea] \quad (5a)$$

$$\Delta G^{\circ\ddagger}_{12} = \Delta G^{\circ\ddagger}_{12}(H_2O) - m^{\ddagger}_{12,urea}[urea] \quad (5b)$$

$$\Delta G^{\circ\ddagger}_{21} = \Delta G^{\circ\ddagger}_{21}(H_2O) - m^{\ddagger}_{21,urea}[urea] \quad (5c)$$

where $\Delta G^\circ(H_2O)$ is the free energy difference between U and Ia in the absence of denaturant, $\Delta G^{\circ\ddagger}_{12}(H_2O)$ and $\Delta G^{\circ\ddagger}_{21}(H_2O)$ are the activation free energies in the absence of denaturant for folding and unfolding reactions, respectively, m_{urea} is the dependence of the equilibrium free energy on urea concentration, $\partial\Delta G^\circ/\partial[urea]$, and $m^{\ddagger}_{12,urea}$ and $m^{\ddagger}_{21,urea}$ are the dependences of the activation free energies on urea concentration for folding and unfolding, $\partial\Delta G^{\circ\ddagger}_{12}/\partial[urea]$ and $\partial\Delta G^{\circ\ddagger}_{21}/\partial[urea]$, respectively. In a two-state model, equilibrium and kinetic parameters are linked by simple relationships:

$$\Delta G^\circ = \Delta G^{\circ\ddagger}_{21} - \Delta G^{\circ\ddagger}_{12} \quad (6a)$$

$$m_{urea} = m^{\ddagger}_{21,urea} - m^{\ddagger}_{12,urea} \quad (6b)$$

Kinetic data and equilibrium data were fitted together to a two-state model by using SIGMAPLOT (Jandel, San Rafael, CA) and the following equations for kinetic and equilibrium data:

$$\lambda = k_{12}(H_2O)\exp\left(\frac{m^{\ddagger}_{12}[urea]}{RT}\right) + k_{21}(H_2O)\exp\left(\frac{m^{\ddagger}_{21}[urea]}{RT}\right) \quad (7)$$

$$CD = \left[(CD_{Ia} + m_{CD,Ia}[urea]) + (CD_U + m_{CD,U}[urea])\exp\left(-\frac{\Delta G^\circ(H_2O)}{RT} + \frac{m_{urea}[urea]}{RT}\right)\right] \Big/ \left[1 + \exp\left(-\frac{\Delta G^\circ(H_2O)}{RT} + \frac{m_{urea}[urea]}{RT}\right)\right] \quad (8)$$

where CD_U and CD_{Ia} are the CD values at 222 nm of U and I_a at 0 M urea and $m_{CD,U}$ and $m_{CD,Ia}$ are the slopes of the linear baselines for the variation of the CD signal of U and Ia with urea concentration, respectively. The baseline for Ia in the transitions monitored by CD was fitted on the final part of the curve measured in the presence of 1 M sucrose and kept constant in the global fitting procedure ($m_{CD,Ia}$ = 6.61 deg·cm^2·dmol^{-1}·M^{-1}). The baseline for U was fitted on the initial part of the curve measured in the absence of sucrose and kept constant in the global fitting procedure ($m_{CD,U}$ = 9.09 deg·cm^2·dmol^{-1}·M^{-1}). The values of $m^{\ddagger}_{12}$ and $m^{\ddagger}_{21}$ found in the absence of sucrose were kept constant in the combined fitting procedure in the presence of varying sucrose and glycerol concentrations.

The viscosities of sucrose, glycerol, and urea solutions were obtained from the literature (*66*−*68*). The variation of solution viscosity with sucrose molarity has been measured at various temperatures, including 5 °C (*67*). For relative viscosities (η/η_0) below 4, the plot of viscosity versus sucrose molarity is perfectly fitted with a single exponential function:

$$\eta/\eta_0 = 1\exp(a[cosolvent]) \quad (9)$$

with an exponential coefficient (a) of 1.25 ± 0.03 at 5 °C. For glycerol, the variation of viscosity with molarity is known at 20 °C but not at 5 °C. With sucrose, solution viscosity at 5 °C differs from that at 20 °C by about 5%, and the data for glycerol at 20 °C were modified accordingly. For $\eta/\eta_0 < 4$, the plot of viscosity versus glycerol molarity is also perfectly fitted with a single exponential function and an exponential coefficient of 0.28 ± 0.01.

RESULTS

Effects of Cosolvents on the Structure of the pH 4 Molten Globule Intermediate. Adding sucrose at pH 4.2 increases the average helical content of I as measured by far-UV circular dichroism (CD) (Figure 1A) but also that of the native form N at pH 6.0 and that of the urea-induced unfolded form U at pH 4.2 (Figure 1B). Conversely, adding sucrose to holo-Mb at pH 6.0 produces no change in the CD spectrum (data not shown). At pH 4.2, the increase in secondary structure content is similar for both intermediate and urea-unfolded forms and is not accompanied by the formation of native tertiary structure as shown by near-UV CD and ^{1}H 1D NMR spectroscopies (Figure 2). The near-UV CD spectrum of native apoMb (N) is characterized by the presence of a dichroic band near 295 nm which is absent in the near-UV CD spectrum of I. Addition of sucrose at pH 4.2 produces a slight increase of the intensity of the near-UV CD signal but not the appearance of a band near 295 nm (Figure 2A). The ^{1}H 1D NMR spectrum at pH 6.0 exhibits chemical shift dispersion and resonance broadening typical of a folded protein as well as upfield-shifted resonances from methyl protons (trace 1 in Figure 2B). At pH 4.2, the ^{1}H 1D NMR spectrum exhibits poor chemical shift dispersion and broad resonances typical of molten globule intermediates and shows no upfield-shifted resonances (trace 2 in Figure 2B). Upon addition of 0.5 or 1.0 M sucrose the ^{1}H 1D NMR spectrum of I conserves the characteristic of a molten globule state although sucrose modifies the dynamical properties of the protein as seen by the disappearance of resonances, line shifts, and line broadening (traces 3 and 4 in Figure 2B).

Effects of Cosolvents on the Thermodynamic Stability of the pH 4 Intermediate. Various small cosolvents, including sucrose, glycerol, sarcosine, and TMAO, increase the stability

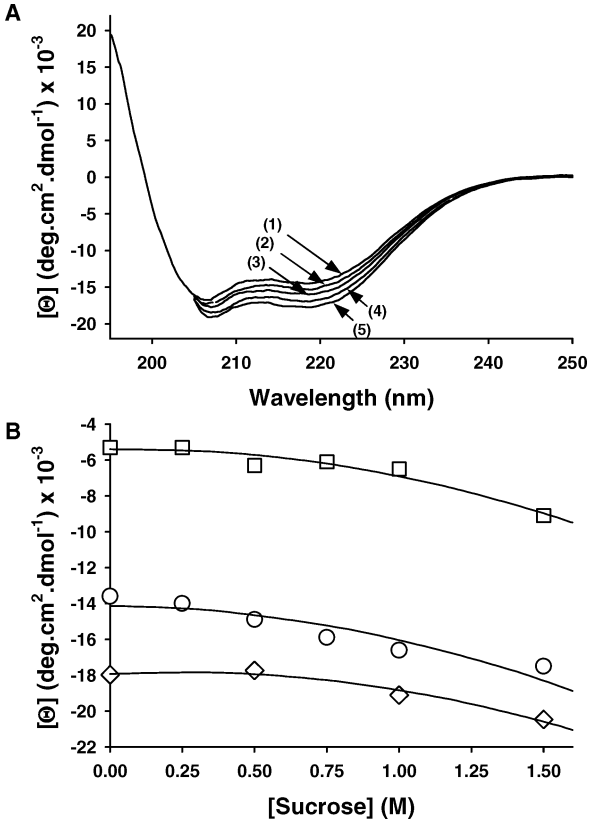

FIGURE 1: Effects of sucrose on the secondary structure content of the sperm whale apoMb pH 4 molten globule intermediate. (A) Far-UV circular dichroism spectra at varying sucrose concentrations. The curves show the far-UV CD spectrum at pH 4.2 in the presence of 0.00 M (1), 0.25 M (2), 0.50 (3), 0.75 (4), and 1.00 M (5) sucrose. In the presence of sucrose, the high absorbance of the solution below 205 nm prevents CD measurement. (B) Average molar ellipticity per residue measured at 222 nm as a function of sucrose concentration. The circles are for the intermediate at pH 4.2, the squares for the urea-unfolded protein at pH 4.2, and the diamonds for the native protein at pH 6. The values for the urea-unfolded form at pH 4.2 are taken from the global fitting procedure described in the text. The lines, showing fits to a second-order polynomial equation, are drawn for the clarity of the figure. Conditions: 2 mM sodium citrate, 30 mM NaCl, pH 4.2, 5 °C. The protein concentration was 1 μM, and the path length was 1 mm.

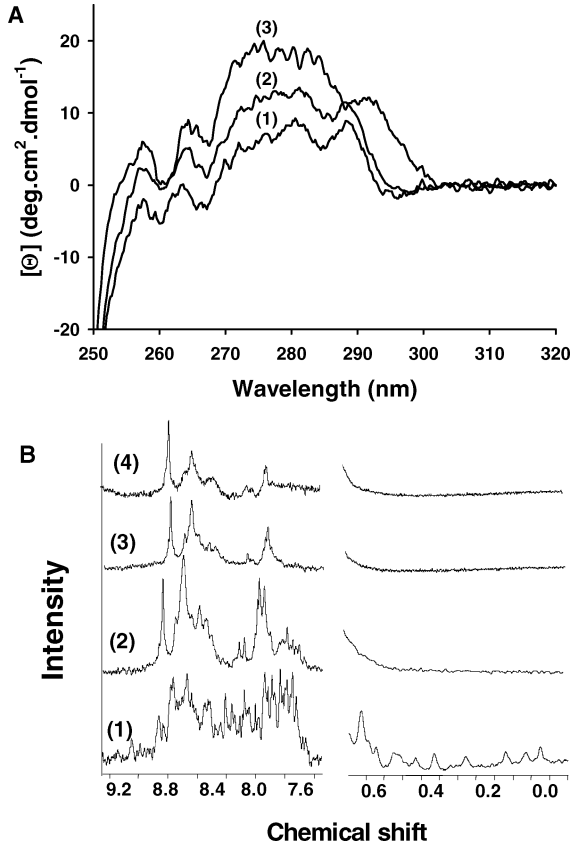

FIGURE 2: Effects of sucrose on the tertiary structure of the sperm whale apoMb pH 4 molten globule intermediate. (A) Near-UV CD spectra at varying sucrose concentrations. The figure shows the spectrum of the molten globule intermediate at pH 4.2 in the absence (1) and presence (2) of 1 M sucrose and the spectrum of the native form N at pH 6.0 (3). Conditions: 2 mM sodium citrate, 30 mM NaCl, pH 4.2 or 6.0, 5 °C. the protein concentration was 100 μM, and the path length was 10 mm. (B) ^{1}H 1D NMR spectra at varying sucrose concentrations. The figure shows the amide region from 6.5 to 9.3 ppm and the upfield region from −0.5 to 0.7 ppm of the ^{1}H 1D NMR spectrum for different forms of sperm whale apoMb: the native form N at pH 5.7 in the absence of sucrose (1) and the intermediate at pH 4.2 in the absence of sucrose (2) and in the presence of 0.5 M (3) and 1.0 M (4) sucrose. Conditions: 5 mM acetate buffer, pH 4.2 or 5.7, 10% D_2O, 25 °C. The protein concentration was 100 μM.

of apoMb pH 4 intermediate Ia relative to the urea-induced unfolded form as seen by a shift of the transition midpoint with cosolvent concentration (Figures 3, 4A, and 5A). The thermodynamic stability of Ia was determined by fitting the urea-induced unfolding transitions to a simple two-state model, using the linear extrapolation method (LEM) (*69*) (Figures 4A and 5A). The m_{urea} value for urea unfolding, ($\partial\Delta G°/\partial$[urea]), does not change with sucrose or glycerol concentration, and therefore, the concerted shift of the transition midpoint (C_m) observed for transitions monitored by Trp fluorescence and by far-UV CD indicates that folding of the intermediate remains cooperative in the presence of these cosolvents (Figure 3).

Effects of Cosolvents on Folding and Unfolding Kinetics of the pH 4 Intermediate. In the absence of cosolvent, the kinetics of the U ⇌ Ia reaction measured within the urea-induced unfolding transition at pH 4.2 were modeled as an apparent two-state process (*57, 59*). Here, folding and unfolding kinetics were measured by stopped-flow Trp fluorescence in the presence of varying concentrations of sucrose or glycerol. The kinetics of the U ⇌ Ia reaction at pH 4.2 are independent of protein concentration in the absence (*59*) as well as in the presence of cosolvent (data not shown). Within the urea-induced transition, a single kinetic phase is observed, and its apparent rate constant exhibits a typical chevron plot at each sucrose or glycerol concentration (Figures 4B and 5B). The apparent rate constant (λ) measured in refolding conditions increases with increasing cosolvent concentrations, whereas that measured in unfolding conditions decreases with increasing cosolvent concentrations. Using the LEM approximation for the dependence of the activation free energies on urea concentration, the kinetic data together with the Trp fluorescence and CD equilibrium data were fitted to a simple two-state model at each sucrose or glycerol concentration (Figures 4 and 5 and Tables 1 and 2). The apparent kinetic *m* values for urea ($m^{‡}_{12,urea}$ and $m^{‡}_{21,urea}$) are not modified by the presence of sucrose or glycerol and remain in agreement with the equilibrium m_{urea} value measured in equilibrium experiments (Tables 1 and 2).

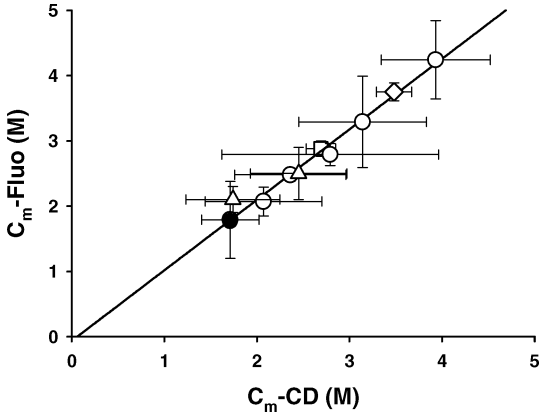

FIGURE 3: C_m values from urea-induced unfolding transitions of sperm whale apoMb at pH 4.2 in the presence of various cosolvents. The C_m values obtained from urea-induced unfolding transitions at pH 4.2 monitored by Trp fluorescence are plotted as a function of the C_m values obtained from urea-induced unfolding transitions monitored by far-UV CD in the same conditions. The closed circle is for the protein in the absence of cosolute. The open circles are for sucrose at concentrations ranging from 0.25 to 1.5 M, the open triangles are for glycerol at 1.1 to 2.1 M, the open square is for 1 M sarcosine, and the open diamond is for 1 M TMAO. Equilibrium transitions monitored by both probes were fitted independently using the LEM approximation. The line shows the linear fit of the data with a slope of 1.08 ± 0.04 (correlation coefficient of 0.993). Conditions: 2 mM sodium citrate, 30 mM NaCl, pH 4.2, 5 °C. The protein concentration was 1 μM.

Folding and Unfolding Kinetics at Constant Stability. A simple test to separate the viscosity effect of a cosolvent from its stabilizing effect is to compare the apparent folding rate under conditions of isostability, in which the stabilizing effect of the cosolvent is matched by the addition of a denaturant (*39*, *40*). Three isostability conditions were considered in our analysis: (1) a condition in which the intermediate is 1200 cal·mol^{-1} more stable than U, corresponding to a fraction of Ia = 0.9, (2) a condition corresponding to the midpoint of the transition (fraction of Ia = 0.5), and (3) a condition in which the intermediate is 1200 cal·mol^{-1} less stable than U, corresponding to a fraction of Ia = 0.1. In each condition, the apparent rate constant for the U ⇌ Ia reaction, λ, as well as the individual folding (k_{12}) and unfolding (k_{21}) rate constants derived from the two-state analysis decrease with increasing cosolvent concentration (data not shown). The plot of the relative rate constant, λ/λ_0, versus cosolvent concentration, where λ_0 is the apparent rate constant in the absence of cosolvent, fits an exponential function (eq 9) with coefficients of 1.14 ± 0.02 and 0.15 ± 0.01 M^{-1} for sucrose and glycerol, respectively. These values are in good agreement with the coefficients 1.22 ± 0.03 and 0.28 ± 0.01 M^{-1} obtained from the fit of relative viscosity as a function of sucrose or glycerol concentration, respectively (Figure 6A). The largest discrepancy observed with glycerol could arise from the precision with which glycerol solutions are prepared. All data align on a plot of the relative rate constant, λ/λ_0, versus the inverse of solvent viscosity, η_0/η, with a slope of 1.00 ± 0.06 and a correlation coefficient of 0.95 (Figure 6B). The effect of viscosity is purely kinetic since the same dependence is found for apparent rate constants measured under refolding or unfolding conditions and is not specific since similar dependences on solvent viscosity are found with sucrose and glycerol.

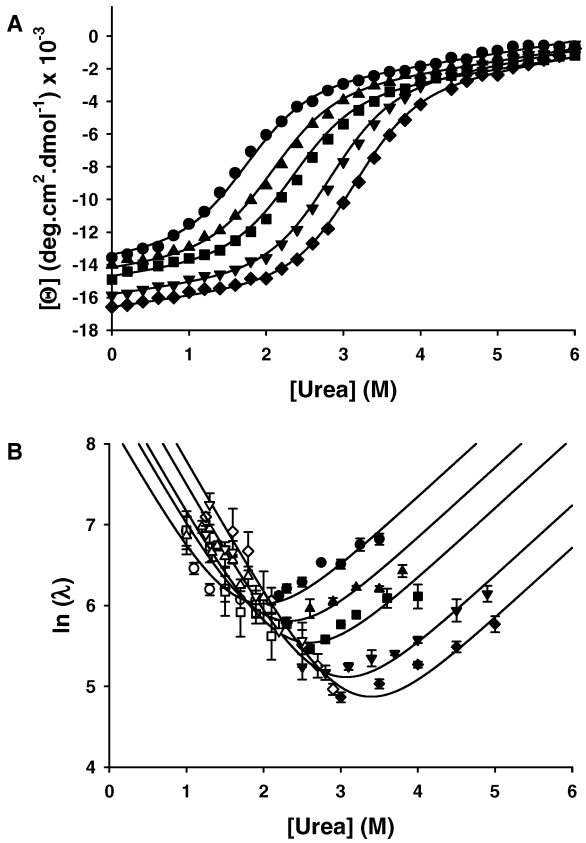

FIGURE 4: Effects of sucrose on the equilibrium stability and on the folding/unfolding kinetics of sperm whale apoMb at pH 4.2. (A) Equilibrium urea-induced unfolding transition in the presence of 0.00 (●), 0.25 (▲), 0.50 (■), 0.75 (▼), and 1.00 (◆) M sucrose. Experiments were followed by molar ellipticity at 222 nm. The lines are drawn according to eq 8 derived from the two-state model and using the parameters presented in Table 1. (B) Apparent rate constant for folding and unfolding kinetics measured in the presence of 0.00 (○, ●), 0.25 (△, ▲), 0.50 (□, ■), 0.75 (▽, ▼), and 1.00 (◇, ◆) M sucrose. The starting material for refolding experiments is U in 4 M urea or higher depending on sucrose concentration, and for unfolding experiments it is a mixture of Ia and Ib at pH 4.2 in 0 M urea. The final protein concentration is between 10 and 20 μM. Stopped-flow fluorescence was monitored with an excitation at 288 nm and a cutoff filter at 305 nm for the emission. Folding and unfolding kinetics were fitted to a one-exponential equation. Each data point is an average of at least three measurements, and each measurement is an average of 4−10 shots. The error bars show standard deviation. The open symbols are for refolding kinetics and the closed symbols for unfolding kinetics. The lines are drawn according to eq 7 derived from the two-state model and using parameters presented in Table 1. Conditions: 2 mM sodium citrate, 30 mM NaCl, pH 4.2, 5 °C.

Folding and Unfolding Kinetics at Constant Viscosity. Solution viscosity depends on cosolvent concentration and temperature. The kinetics presented here were measured at 5 °C. The dependences of solution viscosity on sucrose (*67*) and urea concentration (*66*) are available at this temperature. Assuming independent effects of urea and sucrose on solution viscosity, corrected rate constants are obtained, in agreement with Kramers' theory, by multiplying the measured rate constants by the relative viscosities of both cosolvents:

$$\lambda_{corr} = \lambda(\eta/\eta_0)_{sucrose}(\eta/\eta_0)_{urea} \quad (10)$$

Figure 7A shows the fitted curves of Figure 4B corrected for both sucrose and urea viscosities. The change in stability

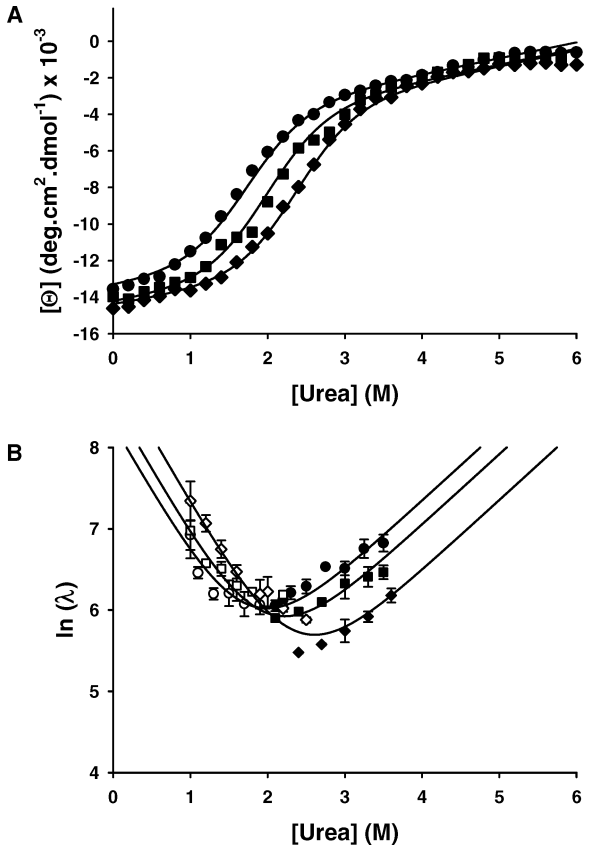

FIGURE 5: Effects of glycerol on the equilibrium stability and folding/unfolding kinetics of sperm whale apoMb at pH 4.2. (A) Equilibrium urea-induced unfolding transition in the presence of 0.00 (●), 1.07 (■), and 2.12 (◆) M glycerol. Experiments were followed by molar ellipticity at 222 nm. The lines are drawn according to eq 8 derived from the two-state model and using parameters presented in Table 2. (B) Observed rate constant for folding and unfolding kinetics measured in the presence of 0.00 (●), 1.07 (■), and 2.12 (◆) M sucrose. Conditions similar to those described in Figure 4B were used. The open symbols are for refolding kinetics and the closed symbols for unfolding kinetics. The lines are drawn according to eq 7 derived from the two-state model and using parameters presented in Table 2.

of Ia now results from a larger change in the refolding rate constant than in the unfolding rate constant.

Using these corrected values, the position of the transition state in terms of burial of accessible surface can be estimated by calculating an α value from the kinetic and equilibrium m values. Alternatively, the α value can be obtained from a plot of the logarithm of the refolding rate constant (k_{12}) versus the logarithm of the inverse of the equilibrium constant for unfolding as shown by eqs 11 and 12:

$$\alpha_{urea} = \frac{m^{\ddagger}_{12,urea}}{m_{urea}} = \frac{\partial \Delta G^{\circ\ddagger}_{12}/\partial[urea]}{\partial \Delta G^{\circ}/\partial[urea]} = \frac{\partial \log k_{12}}{\partial \log(1/K)} \quad (11)$$

$$\alpha_{sucrose} = \frac{m^{\ddagger}_{12,sucrose}}{m_{sucrose}} = \frac{\partial \Delta G^{\circ\ddagger}_{12}/\partial[sucrose]}{\partial \Delta G^{\circ}/\partial[sucrose]} = \frac{\partial \log k_{12}}{\partial \log(1/K)} \quad (12)$$

The α_{urea} value is also known as Tanford's β value (*65*). A value of 0.67 ± 0.05 is calculated here for the U ⇌ Ia reaction at pH 4.2 in the presence of varying sucrose concentration. The effect of urea on solution viscosity is rather small, and an almost identical $\alpha_{urea} = 0.66$ is found with uncorrected kinetic and equilibrium *m* values. With a stabilizing cosolvent, such as sucrose, the effect on solution viscosity is stronger, and corrected kinetics and equilibrium parameters must be used for calculating $\alpha_{sucrose}$. An $\alpha_{sucrose}$ of 0.67 ± 0.02 is obtained by plotting the logarithm of the corrected refolding rate constant (k_{12}) versus the logarithm of the inverse of the corrected equilibrium constant (Figure 7B). A similar value is obtained from the secondary analysis of the corrected unfolding free energies [$\Delta G^{\circ}(H_2O)$] and folding activation free energies [$\Delta G^{\circ\ddagger}_{12}(H_2O)$] extrapolated to zero molar urea that yields kinetic and equilibrium *m* values for sucrose ($m^{\ddagger}_{12,sucrose} = -640 \pm 40$ cal·mol^{-1}·M^{-1}; $m^{\ddagger}_{21,sucrose} = 1330 \pm 45$ cal·mol^{-1}·M^{-1}; $m_{sucrose} = 1980 \pm 100$ cal·mol^{-1}·M^{-1}) (data not shown).

The viscosity of water and urea solutions strongly depends on temperature (*66*, *68*). For diffusion-controlled reactions, temperature dependences of rate constants must be corrected for this effect. Recently, we reported that the rate of the U ⇌ Ia reaction measured near the midpoint of the urea-induced unfolding transition strongly depends on temperature and follows an Arrhenius behavior between 5 and 20 °C with an apparent activation energy of 22300 ± 1400 cal·mol^{-1} (*59*). After correction for the strong temperature dependences of water and urea viscosities (*23*, *25*), the activation energy is 13100 ± 1600 cal·mol^{-1}, showing that the diffusion-controlled formation of Ia is also limited in rate by an energy barrier.

DISCUSSION

Viscosity Dependence of the Folding and Unfolding Kinetics of Ia at pH 4.2. Urea-induced folding and unfolding kinetics of the sperm whale apoMb intermediate are measurable by stopped flow at pH 4 (*57*, *59*). Within the urea-induced unfolding transition, kinetics are monoexponential and exhibit many features of a two-state process. To test whether this reaction is controlled by diffusion, we have measured the effect of solvent viscosity on these reaction rates. The conjunction of both stabilizing and viscogenic effects of small cosolvents produces a paradoxical increase of the folding rate with increasing viscosity, which rather suggests independence on solvent viscosity. However, application of the isostability test reveals a unitary linear dependence of the apparent rate constant, λ/λ_0, on the inverse of solvent viscosity, η_0/η (Figure 7B), as expected from Kramers' theory for diffusion-controlled reactions (*24*).

Application of the isostability test relies on several assumptions. First, it implies that the cosolvent does not modify the structure of the different forms of the protein. The addition of a stabilizing cosolvent increases the secondary structure content of I at pH 4.2, but a similar increase is seen for the urea-unfolded form at pH 4.2 as well as for the native form at pH 6.0, suggesting that cosolvents do not affect the cooperative core of the intermediate but rather stabilize fluctuating secondary structures outside the ABGH core. Low α-helical content in regions corresponding to D and E helices has been found in I at pH 4.2 by NMR spectroscopy (*50*, *54*), and two types of α-helices, native and solvated α-helices, were identified in native apoMb by a temperature-jump experiment monitored by infrared spectroscopy (*70*). The observation of similar kinetic and

Table 1: Kinetic and Equilibrium Parameters at Varying Sucrose Concentrations

	sucrose concn (M)					
parameter	0.00	0.25	0.50	0.75	1.00	1.50
k_{12} (s^{-1})	3900 ± 800	5500 ± 1300	6600 ± 1000	9400 ± 2200	12700 ± 1600	
k_{21} (s^{-1})	48 ± 10	29 ± 17	18 ± 10	8 ± 9	4.5 ± 3	
$\Delta G°$ (cal·mol^{-1})	2400 ± 700	2900 ± 1800	3300 ± 1900	3900 ± 4500	4400 ± 3000	5500 ± 2200
$m^{\ddagger}_{12,urea}$ (cal·mol^{-1}·M^{-1})	−920 ± 110	−920 ± 120	−920 ± 70	−920 ± 110	−920 ± 40	
$m^{\ddagger}_{21,urea}$ (cal·mol^{-1}·M^{-1})	480 ± 40	480 ± 100	480 ± 130	480 ± 150	480 ± 70	
m_{urea} (cal·mol^{-1}·M^{-1})	1400 ± 150	1400 ± 180	1400 ± 210	1400 ± 230	1400 ± 130	1400 ± 600
CD_{Ia} (deg·cm^2·$dmol^{-1}$)	−13400 ± 600	−14100 ± 800	−14700 ± 500	−15900 ± 1200	−16500 ± 400	−17500 ± 400
CD_U (deg·cm^2·$dmol^{-1}$)	−5300 ± 800	−5300 ± 1700	−6300 ± 1300	−6100 ± 4500	−6500 ± 2000	−9100 ± 8200
R^a	0.995	0.983	0.994	0.975	0.996	0.999

[a] Correlation coefficient.

Table 2: Kinetic and Equilibrium Parameters at Varying Glycerol Concentrations

	glycerol concn (M)		
parameter	0.00	1.07	2.12
k_{12} (s^{-1})	3900 ± 800	5300 ± 1000	7900 ± 1000
k_{21} (s^{-1})	48 ± 10	35 ± 16	20 ± 10
$\Delta G°$ (cal·mol^{-1})	2400 ± 700	2800 ± 1400	3300 ± 1700
$m^{\ddagger}_{12,urea}$ (cal·mol^{-1}·M^{-1})	−920 ± 110	−920 ± 100	−920 ± 60
$m^{\ddagger}_{21,urea}$ (cal·mol^{-1}·M^{-1})	480 ± 40	480 ± 75	480 ± 75
m_{urea} (cal·mol^{-1}·M^{-1})	1400 ± 150	1400 ± 130	1400 ± 100
CD_{Ia} (deg·cm^2·$dmol^{-1}$)	−13400 ± 600	−14200 ± 3900	−14400 ± 4600
CD_U (deg·cm^2·$dmol^{-1}$)	−5300 ± 800	−5600 ± 7200	−5700 ± 10600
R^a	0.995	0.983	0.982

[a] Correlation coefficient.

equilibrium *m* values for urea in the absence and presence of a stabilizing cosolvent confirms that the size of the folded core is not affected by the cosolvent. Near-UV CD and NMR spectroscopies show that stabilizing cosolvents do not induce tight packing of the side chains typical of native proteins. Second, a simple application of the isostability test requires that the reaction follows a two-state model. As shown previously for the U ⇌ Ia reaction in the absence of stabilizing cosolvent, the thermodynamic parameters [$\Delta G°(H_2O)$ and m_{urea}] measured under equilibrium conditions in the presence of sucrose or glycerol are similar to the values calculated from the kinetic parameters [$k_{12}(H_2O)$, $k_{21}(H_2O)$, $m^{\ddagger}_{12,urea}$, and $m^{\ddagger}_{21,urea}$], indicating that the U ⇌ Ia reaction remains highly cooperative in these conditions. Third, the validity of the test requires that stabilizing and denaturing cosolvents interact similarly with the ground states and with the transition state (*71*). This hypothesis was verified with several proteins (*25*, *30*, *37*) but not all (*25*). The similar viscosity dependence found here with sucrose and glycerol (Figure 6B) and the similar values of $\alpha^{\ddagger}_{urea}$ and $\alpha^{\ddagger}_{sucrose}$ certainly argue that it is also verified with apoMb Ia. Additional evidence comes from the chevron shift analysis (*39*). For a simple two-state reaction, a stabilizing agent modifies the apparent rate constant by changing the free energy of the transition state relative to the unfolded and native states, whereas, according to Kramers' theory, a viscogenic agent modifies the preexponential factor of the rate equation. A purely stabilizing agent should accelerate refolding and decelerate unfolding, producing a horizontal shift of the chevron plot without changing the minimal rate constant. A purely viscogenic agent should decelerate both the refolding and unfolding rate constants, producing a vertical shift of the chevron plot without changing the position of the minimal rate constant. After correction of the apparent rate constant for the effect of solvent viscosity (Figure 7A) the remaining effect of sucrose is clearly that predicted for a purely stabilizing effect, namely, a horizontal shift of the chevron plot.

The different models that are typically used as limiting cases of protein folding mechanisms, the random-search nucleation and chain propagation model, the diffusion-collision model, and the hydrophobic collapse model, can account for the control of the reaction rate by diffusion and for the cooperativity of the reaction. However, in apoMb, most of the structural elements are defined by local interactions as shown by predictions of local structure using algorithms such as Linus (*72*) and by the presence of significant α-helical structure in isolated peptides and in the acid unfolded form (*54*, *73*). Folding of Ia is, therefore, certainly best represented by the diffusion-collision model (*2*). In this model, unstable microdomains transiently form in different regions of the protein, diffuse, collide, and eventually coalesce to form stable intermediates. Collisions lead to the formation of observable intermediates only if the newly formed interactions provide enough stability for preventing the dissociation of the microdomains. Incorrect structures cannot be consolidated and disappear rapidly. The diffusion-collision model has been used to simulate apoMb folding kinetics (*74*, *75*), and if adequately parametrized, it predicts the sequential appearance of two different partially structured forms on two different time scales in agreement with our observations (*44*) and with the structure of experimentally observed intermediates (*74*).

Nature of the Kinetic Barrier for the U ⇌ Ia Reaction. Deciphering the nature of the folding kinetic barriers is difficult. Unlike simple chemical reactions, protein folding reactions do not involve discrete covalent bond-making or bond-breaking events but, instead, imply conformational

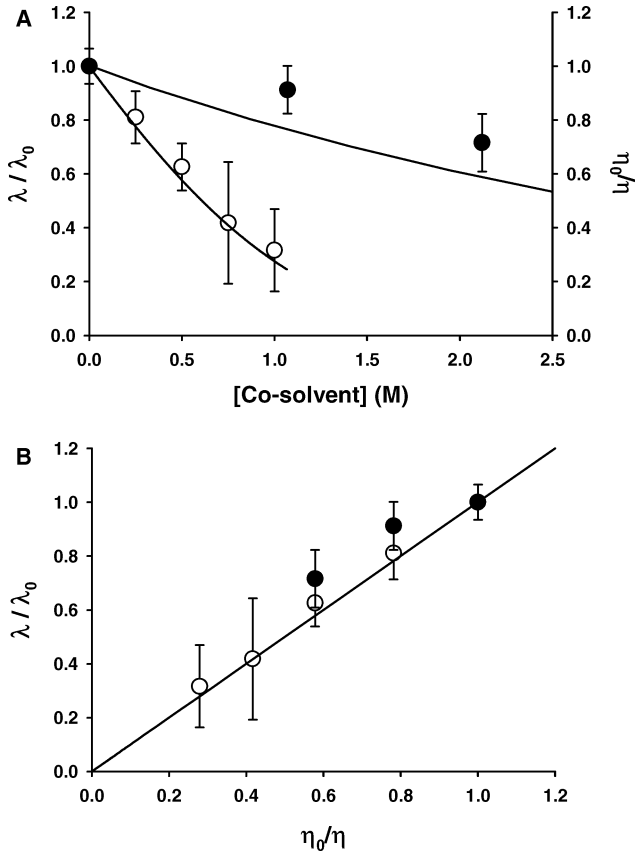

FIGURE 6: Dependence on solvent viscosity. (A) Plot of the relative rate constant (λ_0/λ) at constant stability versus cosolvent concentration. The relative rate constant in isostability condition 2 ($\Delta G° = 0$ kcal·mol^{-1}) is shown here for sperm whale apoMb as a function of the cosolvent concentration. The open circles are for sucrose, and the closed circles are for glycerol. The error bars show standard deviations. Identical curves are obtained in other isostability conditions and are not shown here for the sake of clarity. The lines show the relative viscosity (right axis) as a function of cosolvent concentration. Data for solution viscosity versus sucrose and glycerol molarity are taken from the literature (*67*, *68*). (B) Plot of the relative rate constant (λ_0/λ) at constant stability versus relative viscosity (η/η_0). The line shows the linear regression with a slope of 1.00 ± 0.06 (correlation coefficient, $r^2 = 0.91$). The error bars show standard deviations.

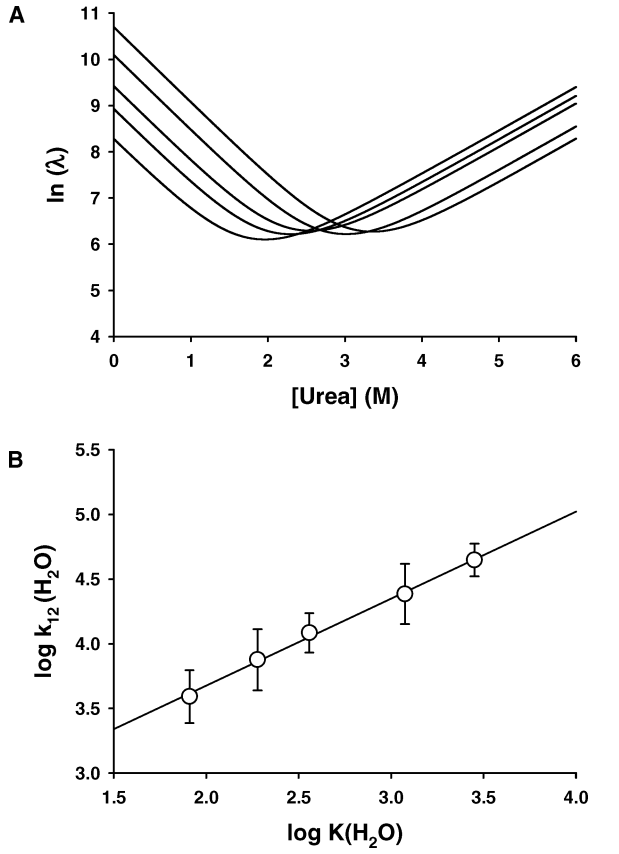

FIGURE 7: Effects of sucrose on the relative stability of the transition state for the U ⇌ Ia reaction. (A) Chevron plots corrected for sucrose viscosity. The fitted curves for the kinetics of sperm whale apoMb in the presence of sucrose (Figure 4B) have been corrected for the viscosity dependence of sucrose and urea using eq 10 and data for sucrose and urea viscosity at 5 °C taken from the literature (*66*, *67*). (B) Plot of log $k_{12}(H_2O)$ versus log($1/K(H_2O)$) at varying sucrose concentrations. The refolding rate constant and the equilibrium constant extrapolated to zero molar urea are corrected for sucrose and urea viscosity. The error bars show standard deviation. The line shows the linear regression with a slope of 0.67 ± 0.02 (correlation coefficient, $r^2 = 0.99$).

diffusion of the protein chain and groups and the making and breaking of numerous noncovalent interactions including interactions that involve solvent molecules. Also, transition states of protein folding reactions are ensembles of conformations rather than of well-defined conformations. The unitary inverse dependence of the folding and unfolding rates of the U ⇌ Ia reaction on solvent viscosity indicates an effect of solvent mobility on protein mobility. To adopt a conformation corresponding to the transition state ensemble of the reaction, the peptide chain must move, and these movements are damped by friction against solvent molecules. The energy barrier for conformational diffusion has been estimated to be in the range of 3.8−6.0 kcal·mol^{-1} for a protein of 60 residues (*76*). In a recent model, the large-scale protein motions involved in protein folding have been linked to fluctuations of the bulk solvent that accounts for the experimentally observed dependence of the reaction rates on solvent viscosity (*77*). In this model, the enthalpic barrier generated by this linkage is also small (<7 kcal·mol^{-1}), whereas the temperature dependence of the apparent folding/unfolding rate constant demonstrates that the U ⇌ Ia reaction is limited in rate by an energy barrier of the order of 13 kcal·mol^{-1}. This enthalpic barrier appears to be higher than that predicted for conformational diffusion and suggests the contributions form other factors such as the breaking of enthalpically favorable protein−protein or protein−solvent interactions or the desolvation of protein groups.

The pH 4 intermediate I consists of an ensemble of compact structures that share a common hydrophobic core formed by the packing of native-like A, B, G, and H helices (*47*, *50*, *54*). I is stabilized by specific and nonspecific hydrophobic side-chain interactions (*52*, *78*) but lacks the tight packing of side chains. The formation of this intermediate requires the concomitant assembly of the N- and C-terminal extremities and their organization in α-helices. Each of these two processes involves motions of the peptide chain through the solvent that can explain the viscosity dependence. In isolation, hydrophobic collapse (*7*, *10*, *11*), collapse driven by intramolecular hydrogen bonds (*79*), and α-helix formation occur faster than the formation of I (*14*, *80*, *81*) and are limited by diffusion as shown by the inverse dependences of their rate on solvent viscosity (*3*, *13*). Multiple lines of evidence indicate that the U ⇌ Ia reaction is a highly cooperative process in which the formation of

the hydrophobic core is concomitant with the formation of α-helices (*57*, *78*, *82*). Recently, we measured similar submillisecond folding and unfolding kinetics by monitoring Trp fluorescence, a probe for hydrophobic collapse, and far-UV CD, a probe for secondary structure formation (*59*). In the folding of apoMb pH 4 from the fully unfolded protein, the tight coupling of these elementary processes thus introduces an additional energy barrier that slows down the overall reaction.

Linear free energy relationships (LFER) are commonly used in organic chemistry to infer the position of the transition state along the reaction coordinate (*83*). Although protein folding reactions are complex processes, LFERs are commonly used to locate the transition state on a reaction coordinate based on accessible surface area (*65*, *84*). The effects of urea and sucrose or of other small cosolvents on protein stability are assigned to preferential binding to or exclusion from protein surface (*60*). These effects are dominated by interactions between the cosolvent and the peptide backbone (*85*−*87*). Sucrose makes unfavorable interactions with the peptide groups and thus stabilizes protein conformations that bury the largest fraction of the peptide groups. Conversely, urea makes favorable interactions with peptide groups and thus favors unfolded conformations, in which peptide groups are most exposed to the solvent. For small globular proteins, the *m* value for denaturing or stabilizing cosolvents is proportional to the change in accessible surface urea (*60*, *88*). The position of the transition state along the reaction coordinates is defined by measuring the effects of a stabilizing (sucrose) or denaturing cosolvent (urea) on the kinetics and equilibria of folding. Since solvent viscosity affects the rate of the U ⇌ Ia reaction, the rate constants must be corrected for this effect before they are used for characterizing the structural properties of the transition state. Failing to apply this correction would lead to a strongly different value of 0.33 for $\alpha^{\ddagger}_{sucrose}$. The value of $\alpha^{\ddagger}_{urea}$ is less dependent on this correction, because changes in solvent viscosity with urea concentration are rather small as compared with those produced by sucrose. After proper correction for solvent viscosity, $\alpha^{\ddagger}_{urea}$ (0.67) perfectly agrees with $\alpha^{\ddagger}_{sucrose}$ (0.67). Although the formation of Ia is limited by diffusion, these α values show that the transition state of the U ⇌ Ia reaction is compact with a high degree of solvent exclusion. About two-thirds (67%) of the peptide groups protected from the solvent in Ia are already buried in the transition state of the reaction. For sperm whale apoMb, the overall change in accessible surface area (ΔASA) upon forming N is 13660 Å^2 (*88*), and the *m* value measured for the U ⇌ Ia reaction (1400 cal·mol^{-1}·M^{-1}) corresponds to a ΔASA of 9330 Å^2 (*88*). Thus, 45% (6200 Å^2) of the total surface buried in the native protein is already buried in the transition state of the U ⇌ Ia reaction.

In this respect, the transition state for the U ⇌ Ia reaction resembles the transition state for the formation of native proteins; namely, the compactness of the transition state is closer to that of the folded form than to that of the unfolded form. α values of ∼0.6−0.7 have been found with a large set of native proteins (*89*), including proteins whose overall folding reaction is controlled by diffusion (*30*, *90*). This suggests that committing a protein to fold requires the burial of roughly two-thirds of the surface area that is buried in the folded form whether this folded form is a native protein or a molten globule intermediate.

Typically, native proteins are also characterized by a large activation enthalpy for unfolding ($\Delta H^{\circ\ddagger}_{unf}$) (*1*). As proposed by Segawa and Sugihara for hen lysozyme, polar cosolvents do not affect the transition state because they cannot penetrate the hydrophobic core (*91*), suggesting that the transition state is formed by breaking interactions and side-chain packing before the solvent can penetrate the structured core and, thus, has properties of a dry molten globule (*92*, *93*). The compactness of the transition state for the U ⇌ Ia reaction suggests a similar process, although Ia is a molten globule intermediate that lacks tight packing of its side chains and is generally assumed to be a "wet" molten globule. The activation enthalpy measured for the U ⇌ Ia reaction is high even after correction for the temperature dependence of solvent viscosity, but it could only be measured near the midpoint of the transition, where the reaction is the slowest. It is thus not possible to determine whether the high-energy barrier controls the folding or the unfolding reaction or both.

ACKNOWLEDGMENT

We thank Jean-Pierre Simorre (Institut de Biologie Structurale, Grenoble) for recording NMR spectra and Buzz Baldwin for comments on the manuscript.

REFERENCES

1. Bilsel, O., and Matthews, C. R. (2000) Barriers in protein folding reactions, *Adv. Protein Chem. 53*, 153−207.
2. Karplus, M., and Weaver, D. L. (1976) Protein-folding dynamics, *Nature 260*, 404−406.
3. Sadqi, M., Lapidus, L. J., and Munoz, V. (2003) How fast is protein hydrophobic collapse?, *Proc. Natl. Acad. Sci. U.S.A. 100*, 12117−12122.
4. Schwarz, G. (1965) On the kinetics of the helix-coil transition of polypeptides in solution, *J. Mol. Biol. 11*, 64−77.
5. Hammes, G. G., and Roberts, P. B. (1969) Dynamics of the helix−coil transition in poly-L-ornithine, *J. Am. Chem. Soc. 91*, 1812−1816.
6. Munoz, V., Thompson, P. A., Hofrichter, J., and Eaton, W. A. (1997) Folding dynamics and mechanism of beta-hairpin formation, *Nature 390*, 196−199.
7. Hagen, S. J., Carswell, C. W., and Sjolander, E. M. (2001) Rate of intrachain contact formation in an unfolded protein: temperature and denaturant effects, *J. Mol. Biol. 305*, 1161−1171.
8. Lapidus, L. J., Eaton, W. A., and Hofrichter, J. (2001) Dynamics of intramolecular contact formation in polypeptides: distance dependence of quenching rates in a room-temperature glass, *Phys. Rev. Lett. 87*, 258101.
9. Buscaglia, M., Kubelka, J., Eaton, W. A., and Hofrichter, J. (2005) Determination of ultrafast protein folding rates from loop formation dynamics, *J. Mol. Biol. 347*, 657−664.
10. Buscaglia, M., Schuler, B., Lapidus, L. J., Eaton, W. A., and Hofrichter, J. (2003) Kinetics of intramolecular contact formation in a denatured protein, *J. Mol. Biol. 332*, 9−12.
11. Krieger, F., Fierz, B., Bieri, O., Drewello, M., and Kiefhaber, T. (2003) Dynamics of unfolded polypeptide chains as model for the earliest steps in protein folding, *J. Mol. Biol. 332*, 265−274.
12. Hagen, S. J., Hofrichter, J., Szabo, A., and Eaton, W. A. (1996) Diffusion-limited contact formation in unfolded cytochrome *c*: estimating the maximum rate of protein folding, *Proc. Natl. Acad. Sci. U.S.A. 93*, 11615−11617.
13. Jas, G. S., Eaton, W. A., and Hofrichter, J. (2001) Effects of viscosity on the kinetics of α-helix and *β*-hairpin formation, *J. Phys. Chem. B 105*, 261−272.
14. Thompson, P. A., Eaton, W. A., and Hofrichter, J. (1997) Laser temperature jump study of the helix ↔ coil kinetics of an alanine peptide interpreted with a "kinetic zipper" model, *Biochemistry 36*, 9200−9210.

15. Arai, M., and Kuwajima, K. (2000) Role of the molten globule state in protein folding, *Adv. Protein Chem. 53*, 209−282.
16. Takahashi, S., Yeh, S. R., Das, T. K., Chan, C. K., Gottfried, D. S., and Rousseau, D. L. (1997) Folding of cytochrome *c* initiated by submillisecond mixing, *Nat. Struct. Biol. 4*, 44−50.
17. Shastry, M. C., and Roder, H. (1998) Evidence for barrier-limited protein folding kinetics on the microsecond time scale, *Nat. Struct. Biol. 5*, 385−392.
18. Uzawa, T., Akiyama, S., Kimura, T., Takahashi, S., Ishimori, K., Morishima, I., and Fujisawa, T. (2004) Collapse and search dynamics of apomyoglobin folding revealed by submillisecond observations of alpha-helical content and compactness, *Proc. Natl. Acad. Sci. U.S.A. 101*, 1171−1176.
19. Roder, H., Maki, K., and Cheng, H. (2006) Early events in protein folding explored by rapid mixing methods, *Chem. Rev. 106*, 1836−1861.
20. Jennings, P. A., and Wright, P. E. (1993) Formation of a molten globule intermediate early in the kinetic folding pathway of apomyoglobin, *Science 262*, 892−896.
21. Chamberlain, A. K., and Marqusee, S. (2000) Comparison of equilibrium and kinetic approaches for determining protein folding mechanisms, *Adv. Protein Chem. 53*, 283−328.
22. Raschke, T. M., and Marqusee, S. (1997) The kinetic folding intermediate of ribonuclease H resembles the acid molten globule and partially unfolded molecules detected under native conditions, *Nat. Struct. Biol. 4*, 298−304.
23. Jacob, M., and Schmid, F. X. (1999) Protein folding as a diffusional process, *Biochemistry 38*, 13773−13779.
24. Kramers, H. A. (1940) Brownian motion in a field of force and the diffusion model of chemical reactions, *Physica 7*, 284−304.
25. Bhattacharyya, R. P., and Sosnick, T. R. (1999) Viscosity dependence of the folding kinetics of a dimeric and monomeric coiled coil, *Biochemistry 38*, 2601−2609.
26. Ansari, A., Jones, C. M., Henry, E. R., Hofrichter, J., and Eaton, W. A. (1992) The role of solvent viscosity in the dynamics of protein conformational changes, *Science 256*, 1796−1798.
27. Kubelka, J., Hofrichter, J., and Eaton, W. A. (2004) The protein folding "speed limit", *Curr. Opin. Struct. Biol. 14*, 76−88.
28. Pabit, S. A., Roder, H., and Hagen, S. J. (2004) Internal friction controls the speed of protein folding from a compact configuration, *Biochemistry 43*, 12532−12538.
29. Qiu, L., and Hagen, S. J. (2004) A limiting speed for protein folding at low solvent viscosity, *J. Am. Chem. Soc. 126*, 3398−3399.
30. Plaxco, K. W., and Baker, D. (1998) Limited internal friction in the rate-limiting step of a two-state protein folding reaction, *Proc. Natl. Acad. Sci. U.S.A. 95*, 13591−13596.
31. Haas, E., Katchalski-Katzir, E., and Steinberg, I. Z. (1978) Effect of the orientation of donor and acceptor on the probability of energy transfer involving electronic transitions of mixed polarization, *Biochemistry 17*, 5064−5070.
32. Qiu, L., Pabit, S. A., Roitberg, A. E., and Hagen, S. J. (2002) Smaller and faster: the 20-residue Trp-cage protein folds in 4 μs, *J. Am. Chem. Soc. 124*, 12952−12953.
33. Klimov, D. K., and Thirumalai, D. (1997) Viscosity dependence of the folding rates of proteins, *Phys. Rev. Lett. 79*, 317−320.
34. Zagrovic, B., and Pande, V. (2003) Solvent viscosity dependence of the folding rate of a small protein: distributed computing study, *J. Comput. Chem. 24*, 1432−1436.
35. Goldberg, J. M., and Baldwin, R. L. (1998) Kinetic mechanism of a partial folding reaction. 2. Nature of the transition state, *Biochemistry 37*, 2556−2563.
36. Waldburger, C. D., Jonsson, T., and Sauer, R. T. (1996) Barriers to protein folding: formation of buried polar interactions is a slow step in acquisition of structure, *Proc. Natl. Acad. Sci. U.S.A. 93*, 2629−2634.
37. Jacob, M., Geeves, M., Holtermann, G., and Schmid, F. X. (1999) Diffusional barrier crossing in a two-state protein folding reaction, *Nat. Struct. Biol. 6*, 923−926.
38. Jacob, M., Schindler, T., Balbach, J., and Schmid, F. X. (1997) Diffusion control in an elementary protein folding reaction, *Proc. Natl. Acad. Sci. U.S.A. 94*, 5622−5627.
39. Matthews, C. R., and Hurle, M. R. (1987) Mutant sequences as probes of protein folding mechanisms, *BioEssays 6*, 254−257.
40. Chrunyk, B. A., and Matthews, C. R. (1990) Role of diffusion in the folding of the alpha subunit of tryptophan synthase from *Escherichia coli*, *Biochemistry 29*, 2149−2154.
41. Teschner, W., Rudolph, R., and Garel, J. R. (1987) Intermediates on the folding pathway of octopine dehydrogenase from *Pecten jacobaeus*, *Biochemistry 26*, 2791−2796.
42. Vaucheret, H., Signon, L., Le Bras, G., and Garel, J. R. (1987) Mechanism of renaturation of a large protein, aspartokinase-homoserine dehydrogenase, *Biochemistry 26*, 2785−2790.
43. Viguera, A. R., and Serrano, L. (1997) Loop length, intramolecular diffusion and protein folding, *Nat. Struct. Biol. 4*, 939−946.
44. Jamin, M., and Baldwin, R. L. (1998) Two forms of the pH 4 folding intermediate of apomyoglobin, *J. Mol. Biol. 276*, 491−504.
45. Nishimura, C., Dyson, H. J., and Wright, P. E. (2006) Identification of native and non-native structure in kinetic folding intermediates of apomyoglobin, *J. Mol. Biol. 355*, 139−156.
46. Tsui, V., Garcia, C., Cavagnero, S., Siuzdak, G., Dyson, H. J., and Wright, P. E. (1999) Quench-flow experiments combined with mass spectrometry show apomyoglobin folds through and obligatory intermediate, *Protein Sci. 8*, 45−49.
47. Hughson, F. M., Wright, P. E., and Baldwin, R. L. (1990) Structural characterization of a partly folded apomyoglobin intermediate, *Science 249*, 1544−1548.
48. Barrick, D., and Baldwin, R. L. (1993) Three-state analysis of sperm whale apomyoglobin folding, *Biochemistry 32*, 3790−3796.
49. Griko, Y. V., Privalov, P. L., Venyaminov, S. Y., and Kutyshenko, V. P. (1988) Thermodynamic study of the apomyoglobin structure, *J. Mol. Biol. 202*, 127−138.
50. Eliezer, D., Chung, J., Dyson, H. J., and Wright, P. E. (2000) Native and non-native secondary structure and dynamics in the pH 4 intermediate of apomyoglobin, *Biochemistry 39*, 2894−2901.
51. Kataoka, M., Nishii, I., Fujisawa, T., Ueki, T., Tokunaga, F., and Goto, Y. (1995) Structural characterization of the molten globule and native states of apomyoglobin by solution X-ray scattering, *J. Mol. Biol. 249*, 215−228.
52. Bertagna, A. M., and Barrick, D. (2004) Nonspecific hydrophobic interactions stabilize an equilibrium intermediate of apomyoglobin at a key position within the AGH region, *Proc. Natl. Acad. Sci. U.S.A. 101*, 12514−12519.
53. Kay, M. S., Ramos, C. H., and Baldwin, R. L. (1999) Specificity of native-like interhelical hydrophobic contacts in the apomyoglobin intermediate, *Proc. Natl. Acad. Sci. U.S.A. 96*, 2007−2012.
54. Eliezer, D., Yao, J., Dyson, H. J., and Wright, P. E. (1998) Structural and dynamic characterization of partially folded states of apomyoglobin and implications for protein folding, *Nat. Struct. Biol. 5*, 148−155.
55. Nishimura, C., Dyson, H. J., and Wright, P. E. (2005) Enhanced picture of protein-folding intermediates using organic solvents in H/D exchange and quench-flow experiments, *Proc. Natl. Acad. Sci. U.S.A. 102*, 4765−4770.
56. Nishimura, C., Dyson, H. J., and Wright, P. E. (2002) The apomyoglobin folding pathway revisited: structural heterogeneity in the kinetic burst phase intermediate, *J. Mol. Biol. 322*, 483−489.
57. Jamin, M., and Baldwin, R. L. (1996) Refolding and unfolding kinetics of the equilibrium folding intermediate of apomyoglobin, *Nat. Struct. Biol. 3*, 613−618.
58. Jamin, M., Yeh, S. R., Rousseau, D. L., and Baldwin, R. L. (1999) Submillisecond unfolding kinetics of apomyoglobin and its pH 4 intermediate, *J. Mol. Biol. 292*, 731−740.
59. Weisbuch, S., Gerard, F., Pasdeloup, M., Cappadoro, J., Dupont, Y., and Jamin, M. (2005) Cooperative sub-millisecond folding kinetics of apomyoglobin pH 4 intermediate, *Biochemistry 44*, 7013−7023.
60. Timasheff, S. N. (1993) The control of protein stability and association by weak interactions with water: how do solvents affect these processes?, *Annu. Rev. Biophys. Biomol. Struct. 22*, 67−97.
61. Edelhoch, H. (1967) Spectroscopic determination of tryptophan and tyrosine in proteins, *Biochemistry 6*, 1948−1954.
62. Piotto, M., Saudek, V., and Sklenar, V. (1992) Gradient-tailored excitation for single quantum NMR spectroscopy of aqueous solutions, *J. Biomol. NMR 2*, 661−665.
63. Hwang, T.-L., and Shaka, A. J. (1995) Water suppression that works. Excitation sculpting using arbitrary waveforms and pulsed field gradients, *J. Magn. Reson. A112*, 275−279.
64. Peterman, B. F. (1979) Measurement of the dead time of a fluorescence stopped-flow instrument, *Anal. Biochem. 93*, 442−444.
65. Tanford, C. (1970) Protein denaturation. C. Theoretical models for the mechanism of denaturation, *Adv. Protein Chem. 24*, 1−95.

66. Perl, D., Jacob, M., Bano, M., Stupak, M., Antalik, M., and Schmid, F. X. (2002) Thermodynamics of a diffusional protein folding reaction, *Biophys. Chem. 96*, 173−190.
67. Sober, H. A. (1970) *Handbook of Biochemistry*, 2nd ed., Chemical Rubber Co., Cleveland, OH.
68. Weast, R. C. (1989) *Handbook of Chemistry and Physics*, 69 ed., CRC Press, Cleveland, OH.
69. Santoro, M. M., and Bolen, D. W. (1988) Unfolding free energy changes determined by the linear extrapolation method. 1. Unfolding of phenylmethanesulfonyl alpha-chymotrypsin using different denaturants, *Biochemistry 27*, 8063−8068.
70. Gilmanshin, R., Williams, S., Callender, R. H., Woodruff, W. H., and Dyer, R. B. (1997) Fast events in protein folding: relaxation dynamics and structure of the I form of apomyoglobin, *Biochemistry 36*, 15006−15012.
71. Ladurner, A. G., and Fersht, A. R. (1999) Upper limit of the time scale for diffusion and chain collapse in chymotrypsin inhibitor 2, *Nat. Struct. Biol. 6*, 28−31.
72. Srinivasan, R., and Rose, G. D. (1995) LINUS: a hierarchic procedure to predict the fold of a protein, *Proteins 22*, 81−99.
73. Reymond, M. T., Merutka, G., Dyson, H. J., and Wright, P. E. (1997) Folding propensities of peptide fragments of myoglobin, *Protein Sci. 6*, 706−716.
74. Pappu, R. V., and Weaver, D. L. (1998) The early folding kinetics of apomyoglobin, *Protein Sci. 7*, 480−490.
75. Bashford, D., Weaver, D. L., and Karplus, M. (1984) Diffusion-collision model for the folding kinetics of the lambda-repressor operator-binding domain, *J. Biomol. Struct. Dyn. 1*, 1243−1255.
76. Wolynes, P., Luthey-Schulten, Z., and Onuchic, J. (1996) Fast-folding experiments and the topography of protein folding energy landscapes, *Chem. Biol. 3*, 425−432.
77. Frauenfelder, H., Fenimore, P. W., Chen, G., and McMahon, B. H. (2006) Protein folding is slaved to solvent motions, *Proc. Natl. Acad. Sci. U.S.A. 103*, 15469−15472.
78. Kay, M. S., and Baldwin, R. L. (1996) Packing interactions in the apomyglobin folding intermediate, *Nat. Struct. Biol. 3*, 439−445.
79. Moglich, A., Joder, K., and Kiefhaber, T. (2006) End-to-end distance distributions and intrachain diffusion constants in unfolded polypeptide chains indicate intramolecular hydrogen bond formation, *Proc. Natl. Acad. Sci. U.S.A. 103*, 12394−12399.
80. Williams, S., Causgrove, T. P., Gilmanshin, R., Fang, K. S., Callender, R. H., Woodruff, W. H., and Dyer, R. B. (1996) Fast events in protein folding: helix melting and formation in a small peptide, *Biochemistry 35*, 691−697.
81. Eaton, W. A., Munoz, V., Hagen, S. J., Jas, G. S., Lapidus, L. J., Henry, E. R., and Hofrichter, J. (2000) Fast kinetics and mechanisms in protein folding, *Annu. Rev. Biophys. Biomol. Struct. 29*, 327−359.
82. Luo, Y., Kay, M. S., and Baldwin, R. L. (1997) Cooperativity of folding of the apomyoglobin pH 4 intermediate studied by glycine and proline mutations, *Nat. Struct. Biol. 4*, 925−930.
83. Maskill, H. (1985) *The Physical Basis of Organic Chemistry*, Oxford University Press, Oxford.
84. Fersht, A. R. (2004) Relationship of Leffler (Bronsted) alpha values and protein folding Phi values to position of transition-state structures on reaction coordinates, *Proc. Natl. Acad. Sci. U.S.A. 101*, 14338−14342.
85. Bolen, D. W., and Baskakov, I. V. (2001) The osmophobic effect: natural selection of a thermodynamic force in protein folding, *J. Mol. Biol. 310*, 955−963.
86. Auton, M., Ferreon, A. C., and Bolen, D. W. (2006) Metrics that differentiate the origins of osmolyte effects on protein stability: a test of the surface tension proposal, *J. Mol. Biol. 361*, 983−992.
87. Street, T. O., Bolen, D. W., and Rose, G. D. (2006) A molecular mechanism for osmolyte-induced protein stability, *Proc. Natl. Acad. Sci. U.S.A. 103*, 13997−14002.
88. Myers, J. K., Pace, C. N., and Scholtz, J. M. (1995) Denaturant m values and heat capacity changes: relation to changes in accessible surface areas of protein unfolding, *Protein Sci. 4*, 2138−2148.
89. Prabhu, N. P., and Bhuyan, A. K. (2006) Prediction of folding rates of small proteins: empirical relations based on length, secondary structure content, residue type, and stability, *Biochemistry 45*, 3805−3812.
90. Schindler, T., and Schmid, F. X. (1996) Thermodynamic properties of an extremely rapid protein folding reaction, *Biochemistry 35*, 16833−16842.
91. Segawa, S., and Sugihara, M. (1984) Characterization of the transition state of lysozyme unfolding. I. Effect of protein-solvent interactions on the transition state, *Biopolymers 23*, 2473−2488.
92. Kiefhaber, T., Labhardt, A. M., and Baldwin, R. L. (1995) Direct NMR evidence for an intermediate preceding the rate-limiting step in the unfolding of ribonuclease A, *Nature 375*, 513−515.
93. Finkelstein, A. V., and Shakhnovich, E. I. (1989) Theory of cooperative transitions in protein molecules. II. Phase diagram for a protein molecule in solution, *Biopolymers 28*, 1681−1694.

BI602574X